

# Stable hopfions in trapped quantum droplets

Zibin Zhao<sup>1,\*</sup>, Guilong Li<sup>1,\*</sup>, Huanbo Luo<sup>1,2,†</sup>, Bin Liu<sup>1,3</sup>, Gui-hua Chen<sup>4,‡</sup>, Boris A. Malomed<sup>5,6</sup>, and Yongyao Li<sup>1,3§</sup>

<sup>1</sup>*School of Physics and Optoelectronic Engineering, Foshan University, Foshan 528000, China*

<sup>2</sup>*Department of Physics, South China University of Technology, Guangzhou 510640, China*

<sup>3</sup>*Guangdong-Hong Kong-Macao Joint Laboratory for Intelligent Micro-Nano Optoelectronic Technology, Foshan University, Foshan 528225, China*

<sup>4</sup>*School of Electronic Engineering & Intelligentization, Dongguan University of Technology, Dongguan 523808, China*

<sup>5</sup>*Department of Physical Electronics, School of Electrical Engineering, Faculty of Engineering, Tel Aviv University, Tel Aviv 69978, Israel*

<sup>6</sup>*Instituto de Alta Investigación, Universidad de Tarapacá, Casilla 7D, Arica, Chile*

Hopfions are a class of three-dimensional (3D) solitons which are built as vortex tori carrying intrinsic twist of the toroidal core. They are characterized by two independent topological charges, *viz.*, vorticity  $S$  and winding number  $M$  of the intrinsic twist, whose product determines the *Hopf number*,  $Q_H = MS$ , which is the basic characteristic of the hopfions. We construct hopfions as solutions of the 3D Gross-Pitaevskii equations (GPEs) for Bose-Einstein condensates in binary atomic gases. The GPE system includes the cubic mean-field self-attraction, competing with the quartic self-repulsive Lee-Huang-Yang (LHY) term, which represents effects of quantum fluctuations around the mean-field state, and a trapping toroidal potential (TP). A systematic numerical analysis demonstrates that families of the states with  $S = 1, M = 0$ , *i.e.*,  $Q_H = 0$ , are stable, provided that the inner TP radius  $R_0$  exceeds a critical value. Furthermore, true hopfions with  $S = 1, M = 1 \sim 7$ , which correspond, accordingly, to  $Q_H = 1 \sim 7$ , also form partly stable families, including the case of the LHY superfluid, in which the nonlinearity is represented solely by the LHY term. On the other hand, the hopfion family is completely unstable in the absence of the LHY term, when only the mean-field nonlinearity is present. We illustrate the knot-like structure of the hopfions by means of an elementary geometric picture. For  $Q_H = 0$ , circles which represent the *preimage* of the full state do not intersect. On the contrary, for  $Q_H \geq 1$  they intersect at points whose number is identical to  $Q_H$ . The intersecting curves form multi-petal structures with the number of petals also equal to  $Q_H$ .

## I. INTRODUCTION

In 1867, Lord Kelvin proposed the hypothesis of vortex atoms [1], sparking mathematical studies of knots. However, it was not until 1997 that Faddeev and Niemi suggested that knots might exist as stable solitons in the three-dimensional classical field theory [2], thereby initiating research of physical realizations of knot-like structures. Numerical studies of the Faddeev-Skyrme version of the O(3) sigma model have demonstrated the existence of stable toroidal solutions in it [3–9]. Unlike ordinary vortex-torus solutions, which are characterized by the single winding number (topological charge)  $M$ , those ones possess two independent winding numbers,  $M$  and  $S$ , with  $S$  determining the *inner twist* of the vortex torus (see Eqs. (14) and (15) below). The corresponding Hopf number is defined as

$$Q_H = MS, \quad (1)$$

which is the fundamental topological characteristic of the intrinsically twisted vortex-soliton states, known as *hopfions*.

Hopfions, which constitute a class of knot-like solitons, may be elegantly presented by dint of the *Hopf fibration*, which is a mapping from the unit sphere in the four-dimensional space onto unit sphere in 3D, *i.e.*,  $S^3 \rightarrow S^2$  [10]. Various species of hopfions have been extensively studied across many fields [11]–[30].

In optics, scalar hopfions with toroidal vortex structures have been proposed as approximate solutions to the Maxwell's equations [31]. Additionally, the use of structured light fields, featuring pronounced spatial variations in their polarization, phase, and amplitude, have made it possible to demonstrate an experimental realization of optical hopfions [32]. Recent studies employing high-order harmonics have also produced optical hopfions [33]. In liquid crystals, material structures in the form of hopfions and various bound states built of them have been widely investigated too, both theoretically and experimentally [34–39]. In cosmology, topological defects are utilized to model the large-scale structure of the universe, with studies of knot-like hopfions providing valuable insights into the topology of cosmic formations [40–44]. These findings highlight the significance of hopfions in unraveling complex topological phenomena across diverse disciplines.

Ultracold atomic Bose-Einstein condensates (BECs), with their tunable intrinsic interactions, offer an expedient platform for the realization of knot-shaped solitons. Various types of vortex knot solitons have been exten-

\* These authors contributed equally to this work.

† huanboluo@fosu.edu.cn

‡ cghphys@gmail.com

§ yongyaoli@gmail.com

sively studied in BECs, including trefoil vortex knots, Solomon vortex links, and various other vortex rings and lines [45–57]. Topological transitions from vortex rings to knots and links were explored too [58]. In particular, encircling a vortex line by a vortex ring gives rise to composite hopfions [59]. Previous studies have demonstrated that hopfions can stably exist in a rotating BEC confined by an oblate harmonic-oscillator trap [59]. Moreover, in the 3D free space, hopfions may be stable in a single-component BEC with self-repulsion whose strength is made spatially modulated, growing, as a function of radial coordinate  $r$ , faster than  $r^3$  [60].

Quantum droplets (QDs), i.e., self-trapped states filled by an ultradilute superfluid, are maintained by the balance between mean-field effects and corrections to them induced by quantum fluctuations [61, 62]. In terms of the corresponding Gross-Pitaevskii equations (GPEs), the corrections are represented by the Lee-Huang-Yang (LHY) terms [63, 64]. Actually, QDs represent a new species of quantum matter, as well as a novel form of self-localized states [65, 66]. Recent detailed studies predict that stable QDs may exist, in the free space, not only in the form of a self-trapped ground-state (GS) mode, but also as robust excited states with embedded vorticity [67–77]. In addition to that, stable vortex QDs with high values of the topological charge (vorticity), as well as multipole QDs, can be maintained by a Gaussian-shaped toroidal potential (TP) [78]. However, three-dimensional (3D) vortex states with complex topological structures, such as hopfions, have yet to be investigated in the realm of QDs.

In this paper, we aim to produce stable solutions for hopfion QDs built with the help of TP. Unlike the above-mentioned one trapping potential, which was employed in Ref. [78], the TP considered here is one of the harmonic-oscillator type, rather than Gaussian-shaped potential structure. Numerical analysis indicates that the hopfions with  $Q_H = 0$  (they may exist with  $M = 0$  and  $S \neq 0$ , see Eq. (1) and Ref. [70], as toroidal patterns whose *preimages* (“skeletons”) [35] are composed of non-intersecting concentric circles) are stable, in a typical experimentally relevant setup, at values of the TP’s inner radius  $R_0 \geq 1.1 \mu\text{m}$ , an instability region appearing below this threshold. Furthermore, hopfions with high values of the Hopf number, up to  $Q_H = 7$ , are also found to be stable. In particular, in contrast to the results of Ref. [59], the inclusion of the LHY term allows for the existence of stable hopfions with  $S = 1$  and  $M > 1$  (hence they have  $Q_H > 1$ , as per Eq. (1)). Similar to the  $Q_H = 0$  solutions, these hopfions exhibit a double-ring pattern, which may serve as an experimental signature for identifying hopfions. These hopfion modes correspond to *preimages* which include intersections. In the horizontal plane, the self-intersecting preimages form petal-like structures, see Fig. 8 below. As  $Q_H$  increases, the number of petals increases accordingly. These findings provide direct insights into the geometric and topological structures of hopfions in QDs and suggest a potential

pathway for their experimental realization.

The subsequent presentation is organized as follows. Section 2 introduces the 3D model including the TP. Numerical results for stationary solutions, including the hopfions with  $Q_H = 0$  and  $Q_H \neq 0$ , are reported in Section 3. Additionally, an elementary geometric representation of the Hopf number is introduced and analyzed in that section. The paper is concluded by Section 4.

## II. THE MODEL

The binary BEC in the 3D space with coordinates  $(X, Y, Z)$  is modeled by the system of nonlinearly-coupled GPEs which include the cubic mean-field terms and quartic LHY ones [61]:

$$i\hbar \frac{\partial}{\partial T} \Psi_1 = -\frac{\hbar^2}{2m} \nabla_{XYZ}^2 \Psi_1 + (G_{11} |\Psi_1|^2 + G_{12} |\Psi_2|^2) \Psi_1 + \Gamma (|\Psi_1|^2 + |\Psi_2|^2)^{\frac{3}{2}} \Psi_1 + V(R, Z) \Psi_1, \quad (2)$$

$$i\hbar \frac{\partial}{\partial T} \Psi_2 = -\frac{\hbar^2}{2m} \nabla_{XYZ}^2 \Psi_2 + (G_{22} |\Psi_2|^2 + G_{21} |\Psi_1|^2) \Psi_2 + \Gamma (|\Psi_1|^2 + |\Psi_2|^2)^{\frac{3}{2}} \Psi_2 + V(R, Z) \Psi_2, \quad (3)$$

where  $G_{11} = G_{22} = 4\pi\hbar^2 a/m$  and  $G_{12} = G_{21} = 4\pi\hbar^2 a'/m$  are the self- and cross-interaction strengths, with atomic mass  $m$ ,  $a$  and  $a'$  being the intra- and inter-species scattering lengths, respectively. The TP potential is defined as

$$V(R, Z) = \frac{1}{2} m \Omega^2 \left[ (R - R_0)^2 + Z^2 \right],$$

where  $R = \sqrt{X^2 + Y^2}$  is the radial coordinate in the 2D plane,  $R_0$  is the inner radius of the toroid, and  $\Omega$  is the TP trapping frequency. The coefficient of the LHY correction is [61]

$$\Gamma = \frac{4m^{\frac{3}{2}} G^{\frac{5}{2}}}{3\pi^2 \hbar^3} = \frac{128\sqrt{\pi}}{3m} \hbar^2 a^{\frac{5}{2}}. \quad (4)$$

For symmetric states with

$$\Psi_1 = \Psi_2 \equiv \Psi/\sqrt{2}, \quad (5)$$

coupled GPEs (2) and (3) admit the reduction to a single equation,

$$i\hbar \frac{\partial}{\partial T} \Psi = -\frac{\hbar^2}{2m} \nabla_{XYZ}^2 \Psi + \frac{\delta G}{2} |\Psi|^2 \Psi + \Gamma |\Psi|^3 \Psi + \frac{1}{2} m \Omega^2 \left[ (R - R_0)^2 + Z^2 \right] \Psi, \quad (6)$$

where  $\delta G = (4\pi\hbar^2/m)(a' + a) \equiv (4\pi\hbar^2/m)\delta a$ . The total number of atoms in the system is

$$N = \int \left( |\Psi_1|^2 + |\Psi_2|^2 \right) d^3\mathbf{R} = \int |\Psi|^2 d^3\mathbf{R}. \quad (7)$$

The set of the system's control parameters includes  $a$ ,  $a'$  and  $N$ .

By means of rescaling,

$$T = t \cdot t_0, (X, Y, Z) = (x, y, z) \cdot l_0, \Psi = l_0^{-\frac{3}{2}} \cdot \psi, \frac{\hbar t_0}{m l_0^2} = 1, \quad (8)$$

where  $t_0$  and  $l_0$  are time and length scales, Eq. (6) is cast in the dimensionless form:

$$i \frac{\partial}{\partial t} \psi = -\frac{1}{2} \nabla^2 \psi + g |\psi|^2 \psi + \gamma |\psi|^3 \psi + \frac{1}{2} \omega \left[ (r - r_0)^2 + z^2 \right] \psi, \quad (9)$$

where we define the scaled strengths of the contact interaction, LHY correction, and TP as, respectively,

$$g = 2\pi \frac{\delta a}{l_0} = 2\pi \delta \tilde{a}, \quad \gamma = \frac{128\sqrt{\pi}}{3} \left( \frac{a}{l_0} \right)^{\frac{5}{2}} = \frac{128\sqrt{\pi}}{3} \tilde{a}^{\frac{5}{2}}, \quad \omega = (t_0 \Omega)^2. \quad (10)$$

In the further analysis, we refer to parameters of the  $^{39}\text{K}$  atomic gas, selecting  $l_0 = 0.1 \mu\text{m}$ . The Hamiltonian (energy) corresponding to Eq. (9) is

$$E = \int \left( \frac{1}{2} |\nabla \psi|^2 + \frac{1}{2} g |\psi|^4 + \frac{2}{5} \gamma |\psi|^5 + \frac{1}{2} \omega \left[ (r - r_0)^2 + z^2 \right] |\psi|^2 \right) d^3\mathbf{r}. \quad (11)$$

Stationary solutions of Eq. (9) with chemical potential  $\mu$  are looked for, below, as

$$\psi = \phi(r) \exp(-i\mu t), \quad (12)$$

with function  $\phi$  obeying the stationary GPE:

$$\mu \phi = -\frac{1}{2} \nabla^2 \phi + g |\phi|^2 \phi + \gamma |\phi|^3 \phi + \frac{1}{2} \omega \left[ (r - r_0)^2 + z^2 \right] \phi. \quad (13)$$

### III. STATIONARY SOLUTIONS

Hopfions are defined as knot-like solitons that can be mapped into the Hopf fibration [79], being characterized by two independent winding numbers [80, 81]. The numerical solution of Eq. (9) for hopfions was performed by

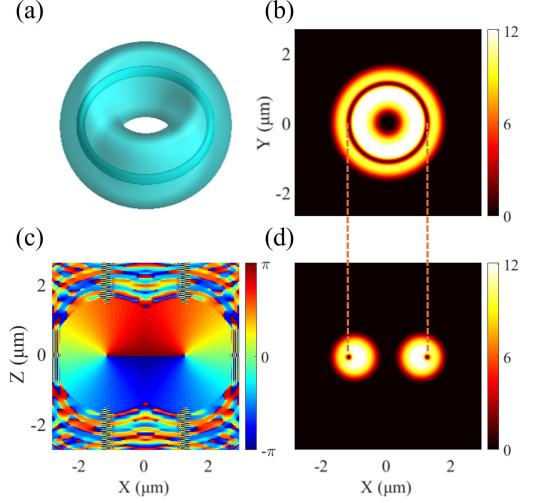


FIG. 1. An example of a stable hopfion with vorticity  $M = 0$ , inner twist  $S = 1$ , trapping frequency  $\Omega = 51000 \text{ Hz}$ , atom number  $N = 55492$ , inner radius  $R_0 = 0.9 \mu\text{m}$ ,  $a = 100a_0$  and  $a' = -110a_0$ . The corresponding dimensionless parameters are  $g = -0.03$ ,  $\gamma = 0.05$ , and  $\omega = 0.1$ . (a) A density isosurface of the stable toroidal vortex. (b) The density distribution in the horizontal plane,  $Z = 0$ . (c-d): The phase and density distributions of the wave function in the vertical plane,  $Y = 0$ . Orange dashed lines designate positions of pivots (phase singularities) of the internal vortex rings, as observed in the  $Y = 0$  plane.

means of the Newton-conjugate-gradient method, starting with the ansatz (initial guess)

$$\phi(r, z) = (r')^S \exp \left( -\frac{(r')^2}{A} + iM\theta + iS\varphi \right), \quad (14)$$

where  $A > 0$  is a real constant and the special coordinates are defined as

$$(r', \theta, \varphi) = \left[ \sqrt{(r - r_0)^2 + z^2}, \arctan \frac{y}{x}, \arctan \frac{r - r_0}{z} \right] \quad (15)$$

(i.e.,  $\theta$  is the usual angular coordinate in the horizontal plane  $(x, y)$ ). In contrast with the usual vortex tori in the 3D space, which feature the single winding number  $M$  (vorticity) in the  $(x, y)$  plane, here the second winding number  $S$ , which is defined in the  $(r, z)$  plane, determines the inner twist of the vortex torus. Ansatz (14) implies a structure like a twisted toroidal vortex tube nested in the 3D solution, coiling up around the vertical ( $z$ ) axis. This shape is typical for solitons of the Faddeev-Skyrme model, with the triplet of real scalar fields realizing the Hopf map,  $\Phi : R^3 \rightarrow S^2$  [2, 3, 82–86], therefore such states are named hopfions, which are characterized by the Hopf number (topological invariant) (Eq. 1).

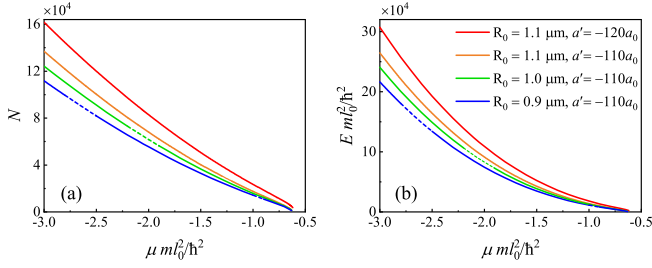


FIG. 2. The total atom number  $N$  and energy  $E$  are plotted vs. the chemical potential  $\mu$  for hopfions with  $S = 1$ ,  $M = 0$  in panels (a) and (b), respectively. Blue and green lines represent hopfions with  $a' = -110 a_0$ ,  $R_0 = 0.9 \mu\text{m}$  and  $R_0 = 1 \mu\text{m}$ , respectively, while the orange and red lines correspond to  $R_0 = 1.1 \mu\text{m}$ ,  $a' = -110 a_0$ , and  $a' = -120 a_0$ , respectively. Solid and dashed segments indicate stable and unstable hopfions, respectively. In all cases, we set  $\Omega = 51000 \text{ Hz}$ ,  $a = 100 a_0$ , the corresponding dimensionless parameters being  $\omega = 0.1$  and  $\gamma = 0.05$ . When  $a' = -110 a_0$  and  $-120 a_0$ , the corresponding dimensionless nonlinearity strength is  $g = -0.03$  and  $-0.06$ , respectively.

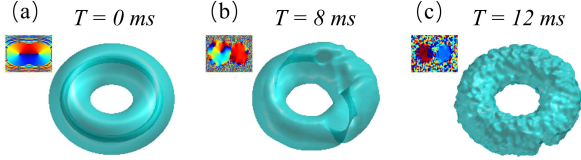


FIG. 3. The unstable evolution of a hopfion with  $S = 1$ ,  $M = 0$ ,  $R_0 = 0.9 \mu\text{m}$ ,  $a = 100 a_0$ ,  $a' = -110 a_0$ , and  $N = 32870$ . Panels (a), (b), and (c) display the hopfions at  $T = 0 \text{ ms}$ ,  $8 \text{ ms}$ , and  $T = 12 \text{ ms}$ , respectively.

### A. Hopfions with $Q_H = 0$

A typical stable hopfion with zero vorticity, i.e.,  $S = 1$ ,  $M = 0$  (hence it has  $Q_H = 0$ , according to Eq. (1)), which is supported by the TP, is displayed in Fig. 1. Direct simulations of its perturbed evolution demonstrate that this hopfion is stable, at least, up to  $T = 10 \text{ ms}$ . Its toroidal shape produces a double-ring pattern in the horizontal plane  $Z = 0$ , as shown in Fig. 1(b), where density  $|\phi|^2$  of the inner ring is slightly higher than in the outer ring. The position of the pivots (phase singularities) of the internal vortex rings at  $Y = 0$ , corresponding to the location of the inner ring, is indicated by the orange dashed line in Fig. 1. This double-ring pattern plays the role similar to that of the hopfion's *preimage* [35], and may serve as a signature for its experimental observation.

Basic properties of the hopfions with  $S = 1$ ,  $M = 0$  are summarized in Fig. 2. It displays the total atom number  $N(\mu)$  and energy  $E(\mu)$  for the hopfions with different values of  $a'$  and  $R_0$ , with solid lines and dashed segments referring to stable and unstable solutions, respectively. It is evident that, for a fixed scattering length  $a$ , increase

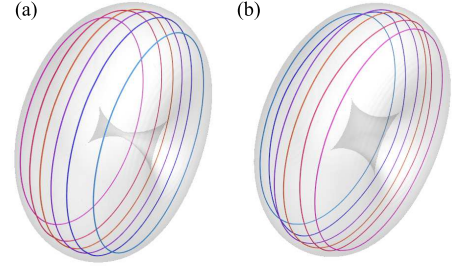


FIG. 4. Isolines of the hopfions with  $S = 1$ ,  $M = 0$ ,  $a = 100 a_0$ ,  $a' = -110 a_0$ ,  $N = 55492$ ,  $R_0 = 0.9 \mu\text{m}$  (a) and  $N = 68006$ ,  $R_0 = 1.1 \mu\text{m}$  (b). Different colors represent different constant values of  $(\text{Re}(\phi), \text{Im}(\phi))$ , which, from right to left, are:  $(0.3, 0.4)$ ,  $(0.5, 0.3)$ ,  $(0.6, 0.1)$ ,  $(0.3, -0.4)$ ,  $(0.5, -0.3)$ , and  $(0.6, -0.1)$ . In (a) and (b), the gray color represent the isosurface with  $|\phi|^2 = 0.4$ .

in the TP radius  $R_0$  leads to higher atom number  $N$  and energy  $E$ . This fact suggests that a larger radius requires a higher number of atoms for the formation of hopfions. Additionally, an instability region arises when  $R_0$  is below  $1.1 \mu\text{m}$ . This observation implies that, for a fixed interaction strength  $g$ , the hopfions suffers destabilization when the inner TP radius  $R_0$  falls below a critical value,  $R_c = 1.1 \mu\text{m}$ . A more detailed investigation reveals that Hopfions with  $S = 1$ ,  $M = 0$  cease to exist when  $R_0$  falls below  $0.4 \mu\text{m}$ . This indicates that in the case of a spherically symmetric harmonic trap, corresponding to  $R_0 = 0$ , such Hopfion structures cannot exist in a stable form.

Note that all the  $N(\mu)$  dependences plotted in Fig. 2(a) satisfy the *Vakhitov-Kolokolov criterion*,  $dN/d\mu < 0$ , which is the well-known necessary stability criterion [88, 89]. On the other hand, it is seen too that the criterion is not sufficient for the full stability, as the curves include unstable segments. The same conclusions are valid for the  $N(\mu)$  dependences for the hopfion families with  $Q_H \neq 0$ , which are plotted below in Fig. 6.

The simulated evolution of an unstable hopfion with  $S = 1$ ,  $M = 0$  is shown in Fig. 3. In the course of the evolution, it loses the phase structure and eventually decay into the GS. Although Fig. 3 illustrates the evolution up to  $T = 12 \text{ ms}$ , the ring-like structure of weakly unstable hopfions can be preserved for a relatively long time and does not split until  $T = 40 \text{ ms}$ . Moreover, for the same values of  $a$  and TP radius  $R_0$ , increase in  $|a'|$ , which corresponds to enhancement of the interaction strength  $g$ , results in an increase in both the number of atoms  $N$  and energy  $E$ . As we adopt  $a' < (-a) < 0$ , it follows from here that we have  $g < 0$ , indicating that the increase of  $|a'|$  strengthens the attractive interaction. Thus, stronger attraction leads to the formation of hopfions with higher atom numbers and energy. Actually, the hopfions with  $S = 1$ ,  $M = 0$  exhibit the lowest atom-number threshold, below which the hopfions do not exist. This threshold increases with the TP radius  $R_0$  and interaction strength  $g$ .

As mentioned above, hopfions are a class of solitons of the Faddeev-Skyrme model and realize the Hopf map,  $\Phi : R^3 \rightarrow S^2$ . For finite-energy solutions, one requires  $\Phi \rightarrow \mathbf{n}$  as  $|\mathbf{r}| \rightarrow \infty$ , where  $\mathbf{n}$  is a constant unit vector. Thus  $R^3$  can be compactified to  $S^3$  and the map reduces to

$$\Phi : S^3 \rightarrow S^2. \quad (16)$$

Since  $\pi_3(S^2) = \mathbb{Z}$ , where different integers from  $\mathbb{Z}$  are the Hopf numbers  $Q_H$ , corresponding to different realizations of the maps [3].

The Hopf number  $Q_H$  also has an elementary geometric interpretation. The *preimage* of every point of the target space  $S^2$  is isomorphic to a circle. These circles are all linked, meaning that any given circle intersects the disk spanned by any other circle. Thus, the Hopf number represents the linkage number, which quantifies the degree of the linkage between any two arbitrary circles [3, 48, 87].

For the hopfions with  $Q_H = 0$ , which we address in this section, different circles corresponding to different points in the parameter space  $S^2$  do not link, resulting in concentric circles. To illustrate this property, Fig. 4 shows contour plots of different hopfions with  $R_0 = 0.9 \mu\text{m}$  and  $1.1 \mu\text{m}$ . Solid circles in the figure represent contours where both the real and imaginary parts of wave function  $\phi$  are constant (i.e.,  $\text{Re}(\phi) = C_1$ ,  $\text{Im}(\phi) = C_2$ ), different colors corresponding to different values of  $C_1$  and  $C_2$ . It is clearly observed that these circles are concentric and do not intersect, which is consistent with  $Q_H = 0$ . The real and imaginary parts of the wave function represent two degrees of freedom in the parameter space  $S^2$ , with different values corresponding to different points on the  $S^2$  sphere. Solid circles in the figure represent the projection of a point from the  $S^2$  sphere onto the real space. The projection is realized through the Hopf map and stereographic projection.

### B. Hopfions with $Q_H \neq 0$

Hopfions with nonzero Hopf numbers are topologically nontrivial states. Examples of hopfions with  $S = 1, M = 1 \sim 7$  are shown in Fig. 5. Accordingly, they carry  $Q_H = 1 \sim 7$ . The first row of Fig. 5 illustrates density isosurfaces of the hopfions, revealing that they all are toroidal modes. The second and third rows display the phase distributions of the wave functions in the horizontal ( $Z = 0$ ) and vertical ( $Y = 0$ ) planes, respectively. The latter rows demonstrate that the hopfions indeed have the twist number  $S = 1$ , while their vorticities in the horizontal plane range from  $M = 1$  to  $M = 7$ . The stability of these hopfions was verified by simulation of their perturbed evolution, in the framework of Eq. (9).

The  $N(\mu)$  and  $E(\mu)$  dependences for hopfions with  $Q_H = 1 \sim 7$  are shown in Fig. 6, where solid and dashed segments again represent stable and unstable solutions, respectively. It is observed that, as the twist winding

number  $M$  increases, the atom number  $N$  and energy  $E$  of the hopfions decrease. Similar to the above results for  $Q_H = 0$ , the hopfions with  $Q_H = 1 \sim 7$  also exhibit a minimum- $N$  threshold, which increases with the value of  $Q_H$ . Hopfions with higher Hopf numbers  $Q_H$  display intermittent instability regions. In general, the instability region becomes broader as the Hopf number increases.

The evolution of unstable hopfions is illustrated in Fig. 7 (a1-a3). It is observed that the unstable hopfions lose their topological structure in the course of the evolution. The vortex ring in the center is gradually destroyed, and the hopfion eventually degenerates into the GS. Similar to the unstable evolution reported in Ref. [59], the vortex ring in the center splits into fragments of vortex lines. Additionally, we examined the evolution of a stable hopfion with parameters  $S = 1, M = 1, \Omega = 51000 \text{ Hz}$ , and  $N = 111130$ . As shown in Fig. 7 (b1-b3), the hopfion becomes unstable when the TP strength falls below the critical value,  $\Omega_c = 15405 \text{ Hz}$ . Furthermore, as displayed in Fig. 7 (c1-c3), if the TP is removed at the start of the evolution, the previously stable hopfion rapidly becomes unstable on a short timescale  $\simeq 0.02 \text{ ms}$ . This observation suggests that the hopfions, characterized by their complex topological structure, are unlikely to remain stable in the free space, without the support of the TP.

Unlike the previously discussed case of  $Q_H = 0$ , where the curves corresponding to constant values of  $(\text{Re}(\phi), \text{Im}(\phi))$  in the 3D space do not intersect, the hopfions with  $Q_H \neq 0$  exhibit intersection of these curves, resulting in a knot with a linking number equal to  $Q_H$ . Figure 8 offers the elementary geometric representations of the hopfions with  $Q_H = 1 \sim 7$ . In the figure, red and blue curves correspond to distinct constant values of  $(\text{Re}(\phi), \text{Im}(\phi))$ . To better highlight the structure of the hopfions, the figure focuses on the shape of the knots in the horizontal plane,  $Z = 0$ , where the linking number can be identified by observing which curve passes over which one. Note that these are 3D curves, but not flat loops. When viewed in the  $Z = 0$  cross-section, these knots exhibit a petal-like structure, with the number of petals increasing with the Hopf number,  $Q_H$ .

It is natural to expect that hopfions with  $Q_H \neq 0$  cannot be stable in the absence of the LHY correction, i.e., setting  $\gamma = 0$  in Eq. (9). Indeed, our numerical analysis readily demonstrates that, while the combination of the mean-field self-attractive cubic nonlinearity and TP trap creates hopfions as solutions of Eq. (9), they are completely unstable. In particular, in the case of  $\gamma = 0$  the dependence  $N(\mu)$  for the hopfion family with  $S = 1, M = 1$  ( $Q_H = 1$ ), displayed in Fig. 9(a) fully contradicts the VK criterion, which confirms its complete instability.

The unstable evolution of the hopfions in this case is illustrated in Fig. 10. It is seen that the unstable hopfion with a relatively small norm suffers complete destruction (in panel (a)), while a hopfion with a large norm splits into a set of fragments, in panel (b).

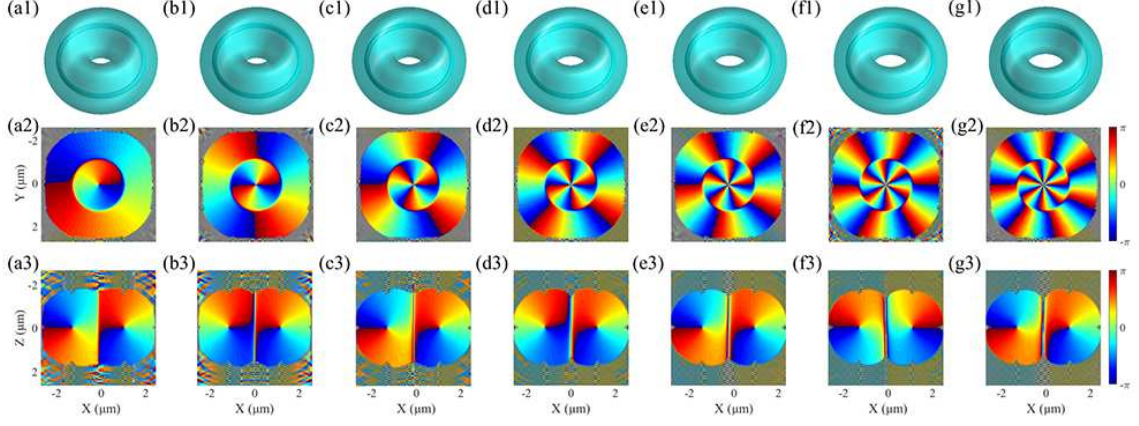


FIG. 5. Stable hopfions with  $S = 1$ ,  $M = 1$  (a1-a3), 2 (b1-b3), 3 (c1-c3), 4 (d1-d3), 5 (e1-e3), 6 (f1-f3), 7 (g1-g3). The first row shows the density isosurface. The second and third rows display the phase of the wave function in the planes  $Z = 0$  and  $Y = 0$ , respectively. The physical parameters are set as  $a = 100 a_0$ ,  $a' = -110 a_0$ ,  $R = 0.9 \mu\text{m}$ ,  $\Omega = 51000 \text{ Hz}$ , and  $N = 111130$  (a1-a3), 109570 (b1-b3), 107240 (c1-c3), 104270 (d1-d3), 100730 (e1-e3), 96706 (f1-f3), 92267 (f1-f3).

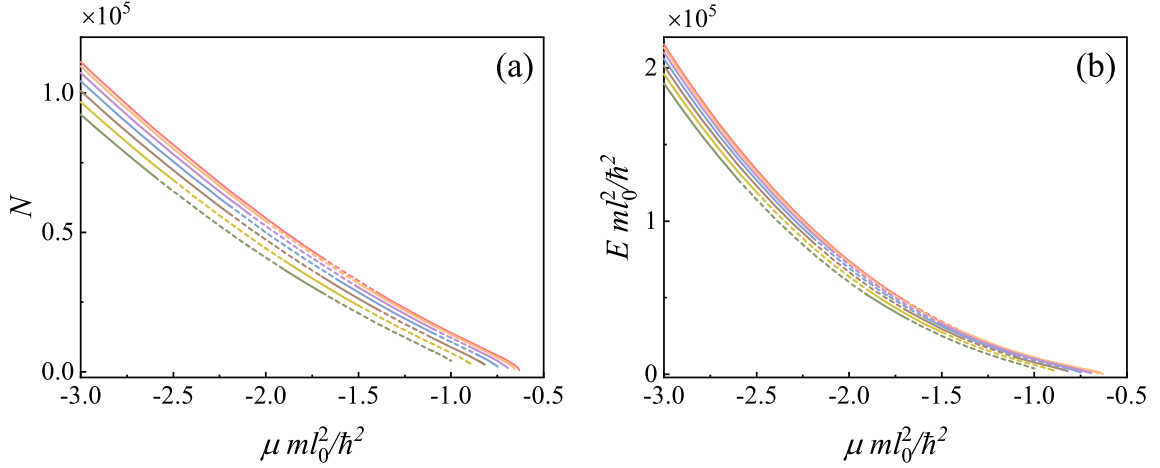


FIG. 6. The atom number  $N$  and energy  $E$  vs. chemical potential  $\mu$  for the hopfions with  $Q_H = 1 \sim 7$ . Solid and dashed segments denote stable and unstable solutions, respectively. The curves, ordered from the top to bottom, correspond to values of the twist topological charge  $M = 1 \sim 7$  in the increasing order, with fixed vorticity  $S = 1$ . The physical parameters are set as  $a = 100 a_0$ ,  $a' = -110 a_0$ ,  $\Omega = 51000 \text{ Hz}$ ,  $R = 0.9 \mu\text{m}$ .

Additionally, we examined the special case in which the nonlinearity is represented solely by the LHY term, i.e.,  $g = 0$  in Eq. (9) (the so-called LHY superfluid [63, 90]). In this case, we find that hopfion families with  $Q_H = 1$  obey the VK criterion and are chiefly stable, including an unstable subfamily, as demonstrated by the blue curves in Fig. 9. The figure also shows that, for the same value of strength  $\gamma$  of the LHY term and  $g = 0$ , the hopfions exhibit lower norm  $N$  and energy  $E$ , in comparison to their counterparts found in the presence of the mean-field self-attraction ( $g < 0$ ). However, the instability region is slightly larger in the case of  $g = 0$  than in the presence of  $g < 0$ .

#### IV. CONCLUSION

The objective of the work is to construct stable QDs (quantum droplets) carrying the highly nontrivial topological structure which makes it possible to identify them as hopfions. The stability of (a part of) these states, which is a crucially important issue, is provided by the action of TP (toroidal potential), which is included in the corresponding system of the 3D GPEs (Gross-Pitaevskii equations). The interaction in the GPE system is represented by the self-attractive mean-field cubic terms and repulsive LHY (Lee-Huang-Yang) quartic ones, which represent the effect of quantum fluctuations around the mean-field configurations. The numerical analysis demonstrates that not only the modes with zero

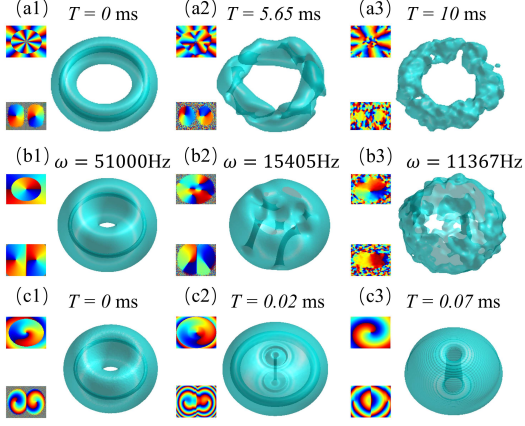


FIG. 7. The unstable evolution of hopfions with  $Q_H \neq 0$ . (a1)-(a3): A perturbed hopfion with  $S = 1$ ,  $M = 7$ ,  $R_0 = 0.9 \mu\text{m}$ ,  $N = 7523$ ,  $a = 100 a_0$ , and  $a' = -110 a_0$ . The evolution of the hopfions with  $S = 1$ ,  $M = 1$ , and  $\Omega = 51000 \text{ Hz}$  under the action of a gradually decreasing TP strength  $\Omega$  is shown in (b1)-(b3). Panels (c1)-(c3) illustrate the evolution of a hopfion after the TP was removed at the start of the evolution, with parameters  $S = 1$ ,  $M = 1$ ,  $R_0 = 0.9 \mu\text{m}$ ,  $N = 111130$ ,  $a = 100 a_0$ , and  $a' = -110 a_0$ .

Hopf number,  $Q_H = 0$  (they have zero vorticity,  $M = 0$ , and the twist topological charge  $S = 1$ ) can stably exist in this system, but also the hopfions in the range of  $Q_H \equiv MS = 1 \sim 7$  exhibit stability regions. The intensity profiles of these solutions in the horizontal ( $Z = 0$ ) plane reveal a characteristic double-ring *preimage* of the hopfion, which may serve as a distinct signature for identifying hopfions in the experiment. Naturally, the stability regions gradually shrink with the increase of  $Q_H$ . In the course of their evolution, unstable hopfions lose their topological structures, eventually decaying into the GS (ground state). The hopfions cannot be stable if the confining TP is absent, i.e., they cannot represent stable states in the free space. To further elucidate the geometry and topology of the hopfions (in particular, of the stable ones), we have displayed their elementary geometric representation by means of the corresponding Hopf map (of the parameter manifold into the real space) and stereographic projection. For  $Q_H = 0$ , the representation reveals a series of non-intersecting concentric rings in the real space. In contrast, the solutions with  $Q_H = 1 \sim 7$  exhibit intricate knots, with the linking number equal to  $Q_H$ . In the horizontal plane, these knots exhibit a petal-like structure, with the number of petals also equal to  $Q_H$ . Furthermore, the role of the LHY term is crucial in determining the stability of Hopfions. When the LHY term is absent ( $g < 0, \gamma = 0$  in Eq. (9)), Hopfions with  $Q_H \neq 0$  cannot stably exist. In contrast, when only the LHY nonlinear term is present ( $g = 0, \gamma \neq 0$  in Eq. (9)), Hopfions with  $Q_H \neq 0$  can stably exist, although the instability region is slightly larger compared to the case

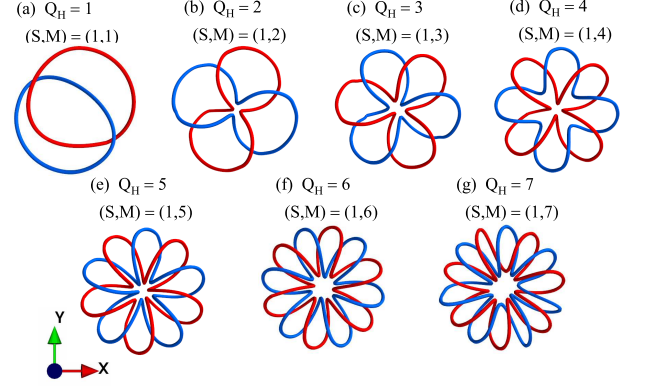


FIG. 8. The elementary geometric interpretation of the Hopf numbers  $Q_H = 1$  (a), 2 (b), 3 (c), 4 (d), 5 (e), 6 (f), and 7 (g) in the horizontal plane,  $Z = 0$ . The red and blue solid curves represent distinct constant values of  $(\text{Re}(\phi), \text{Im}(\phi))$ : for  $Q_H = 1$ , these are  $(2, 2)$  (red) and  $(-2, -2)$  (blue); for  $Q_H = 2$ , these are  $(0.3, 0.4)$  (red) and  $(-0.3, -0.4)$  (blue); for  $Q_H = 3$ , these are  $(-0.3, 0.4)$  (red) and  $(0.3, -0.4)$  (blue); for  $Q_H = 4$ , these are  $(-0.4, -0.3)$  (red) and  $(0.4, 0.3)$  (blue); for  $Q_H = 5$ , these are  $(-0.3, -0.2)$  (red) and  $(0.2, -0.3)$  (blue); for  $Q_H = 6$ , these are  $(-0.3, -0.3)$  (red) and  $(0.3, 0.3)$  (blue); and for  $Q_H = 7$ , these are  $(-0.4, -0.4)$  (red) and  $(0.4, 0.4)$  (blue).

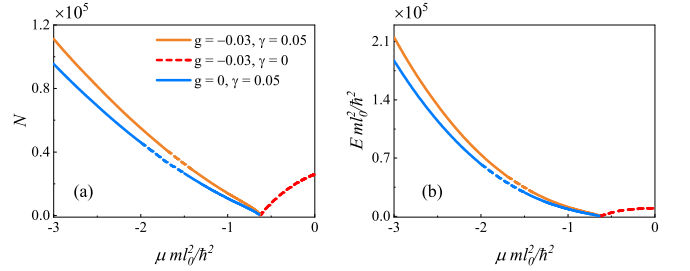


FIG. 9. The  $N(\mu)$  (a) and  $E(\mu)$  (b) curves for hopfion families with  $S = 1$ ,  $M = 1$ . The orange curves represent an example of the generic case considered above, with  $g = -0.03, \gamma = 0.05$ . The red curves represent a fully unstable family in the absence of the LHY term, with  $\gamma = 0$  and  $g = -0.03$ . The blue curves display a partly stable family found in the absence of the mean-field self-attraction, with  $g = 0$  and  $\gamma = 0.05$  (the “LHY superfluid”). Solid and dashed segments correspond to stable and unstable families, respectively.

with  $g < 0$ .

## ACKNOWLEDGMENTS

This work was supported by NNSFC (China) through Grants No. 12274077, 12475014, the Natural Science Foundation of Guangdong province through Grant No. 2024A1515030131, 2025A1515011128, 2023A1515010770, Guangdong Basic and Applied Basic Research Foundation Grant No. 2023A1515110198, the Research Fund of Guangdong-Hong Kong-Macao Joint Laboratory for In-

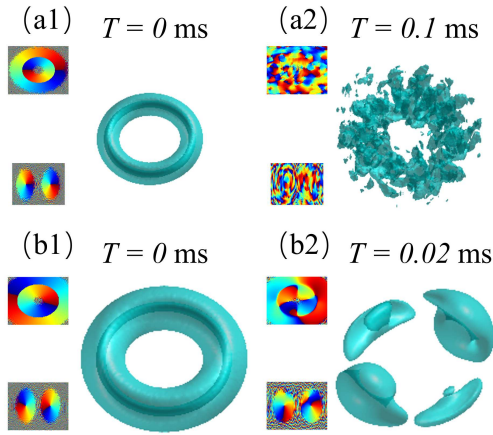


FIG. 10. The unstable evolution of hopfions with  $S = 1$ ,  $M = 1$  in the absence of the LHY term, *viz.*,  $\gamma = 0$  and  $g = -0.03$ . Panels (a1-a2) and (b1-b2) correspond, respectively, to values of the total norm  $N = 25.888$  and  $N = 223$ .

telligent Micro-Nano Optoelectronic Technology through grant No.2020B1212030010. The work of B.A.M. is supported, in part, by the Israel Science Foundation through grant No. 1695/2022.

- 
- [1] W. Thomson, II. On vortex atoms, London, Edinburgh, Dublin Philos. Mag. J. Sci. 34(227), 15-24 (1867) .
  - [2] L. Faddeev and A. J. Niemi, Stable knot-like structures in classical field theory, Nature 387(6628), 58-61 (1997).
  - [3] J. Gladikowski and M. Hellmund, Static solitons with nonzero Hopf number, Phys. Rev. D 56(8), 5194-5199 (1997).
  - [4] R. A. Battye, Knots as Stable Soliton Solutions in a Three-Dimensional Classical Field Theory, Phys. Rev. Lett. 81(22), 4798-4801 (1998).
  - [5] H. Aratyn, L. A. Ferreira, and A. H. Zimerman, Toroidal solitons in 3+1 dimensional integrable theories, Phys. Lett. B 456(2), 162-170 (1999).
  - [6] J. Hietarinta and P. Salo, Faddeev-Hopf knots: dynamics of linked un-knots, Phys. Lett. B 451(1), 60-67 (1999).
  - [7] H. Aratyn, L. A. Ferreira, and A. H. Zimerman, Exact Static Soliton Solutions of ( 3 + 1 ) -Dimensional Integrable Theory with Nonzero Hopf Numbers, Phys. Rev. Lett. 83(9), 1723-1726 (1999).
  - [8] R. S. Ward, Skyrmions and Faddeev-Hopf solitons, Phys. Rev. D 70(6), 061701 (2004).
  - [9] P. Sutcliffe, Knots in the Skyrme-Faddeev model, Proc. R. Soc. A. 463(2087), 3001-3020 (2007).
  - [10] E. Radu and M. S. Volkov, Stationary ring solitons in field theory – Knots and vortons, Phys. Rep. 468(4), 101-151 (2008).
  - [11] B. Göbel, I. Mertig, and O. A. Tretiakov, Beyond skyrmions: Review and perspectives of alternative magnetic quasiparticles, Phys. Rep. 895(12), 1-28 (2021).
  - [12] M. Sallermann, H. Jónsson, and S. Blügel, Stability of hopfions in bulk magnets with competing exchange interactions, Phys. Rev. B 107(10), 104404 (2023).
  - [13] D. Raftrey and P. Fischer, Field-Driven Dynamics of Magnetic Hopfions, Phys. Rev. Lett. 127(25), 257201 (2021).
  - [14] Y. Liu, W. Hou, X. Han, et al., Three-Dimensional Dynamics of a Magnetic Hopfion Driven by Spin Transfer Torque, Phys. Rev. Lett. 124(12), 127204 (2020).
  - [15] S. B. Gudnason and M. Nitta, Baryonic torii: Toroidal baryons in a generalized Skyrme model, Phys. Rev. D 91(4), 045027 (2015).
  - [16] Y. Shen, Q. Zhang, P. Shi, et al., Optical skyrmions and other topological quasiparticles of light, Nat. Photon. 18(1), 15-28 (2024).
  - [17] D. Sugic, R. Droop, E. Otte, et al., Particle-like topologies in light, Nat. Commun. 12(1), 6785 (2021).
  - [18] N. A. Veretenov, S. V. Fedorov, and N. N. Rosanov, Topological Vortex and Knotted Dissipative Optical 3D Solitons Generated by 2D Vortex Solitons, Phys. Rev. Lett. 119(26), 263901 (2017).
  - [19] I. Luk'yanchuk, Y. Tikhonov, A. Razumnaya, et al., Hopfions emerge in ferroelectrics, Nat. Commun. 11(1), 2433 (2020).
  - [20] P. J. Ackerman, Diversity of Knot Solitons in Liquid Crystals Manifested by Linking of Preimages in Torons and Hopfions, Phys. Rev. X 7(1), 011006 (2017).
  - [21] D. Kleckner and W. T. M. Irvine, Creation and dynamics of knotted vortices, Nat. Phys. 9(4), 253-258 (2013).
  - [22] S. Bolognesi, Hopf Skyrmin in QCD with adjoint quarks, Phys. Rev. D 75(6), 065020 (2007).
  - [23] M. Ezawa, Topological semimetals carrying arbitrary Hopf numbers: Fermi surface topologies of a Hopf link, Solomon's knot, trefoil knot, and other linked nodal varieties, Phys. Rev. B 96(4), 041202 (2017).
  - [24] P. Sutcliffe, Hopfions in chiral magnets, J. Phys. A: Math. Theor. 51(37), 375401 (2018).
  - [25] M. Kobayashi and M. Nitta, Torus knots as Hopfions, Phys. Lett. B 728(20), 314-318 (2014).
  - [26] X. S. Wang, A. Qaiumzadeh, and A. Brataas, Current-Driven Dynamics of Magnetic Hopfions, Phys. Rev. Lett. 123(14), 147203 (2019).

- [27] X. Yu, Y. Liu, K. V. Iakoubovskii, et al., Realization and Current-Driven Dynamics of Fractional Hopfions and Their Ensembles in a Helimagnet FeGe, *Adv. Mater.* 35(20), 2210646 (2023).
- [28] D. Ehrmanntraut, R. Droop, D. Sugic, et al., Optical second-order skyrmionic hopfion, *Optica*, 10(6), 725-731 (2023).
- [29] H. Wang and S. Fan, Photonic Spin Hopfions and Monopole Loops, *Phys. Rev. Lett.* 131(26), 263801 (2023).
- [30] F. N. Rybakov, N. S. Kiselev, A. B. Borisov, et al., Magnetic hopfions in solids, *APL Materials* 10(11), 111113 (2022).
- [31] C. Wan, Y. Shen, A. Chong, et al., Scalar optical hopfions, *eLight* 2(1), 22 (2022).
- [32] Y. Shen, B. Yu, H. Wu, et al., Topological transformation and free-space transport of photonic hopfions, *Adv. Photon.* 5(1), 015001 (2023).
- [33] Z. Lyu, Y. Fang, and Y. Liu, Formation and Controlling of Optical Hopfions in High Harmonic Generation, *Phys. Rev. Lett.* 133(13), 133801 (2024).
- [34] P. J. Ackerman, J. van de Lagemaat, and I. I. Smalyukh, Self-assembly and electrostriction of arrays and chains of hopfion articles in chiral liquid crystals, *Nat. Commun.* 6(1), 6012 (2015).
- [35] I. I. Smalyukh, Review: knots and other new topological effects in liquid crystals and colloids, *Rep. Prog. Phys.* 83(10), 106601 (2020).
- [36] J.-S. B. Tai and I. I. Smalyukh, Three-dimensional crystals of adaptive knots, *Science* 365(6460), 1449-1453 (2019).
- [37] J.-S. B. Tai, P. J. Ackerman, and I. I. Smalyukh, Topological transformations of Hopf solitons in chiral ferromagnets and liquid crystals, *Proc. Natl. Acad. Sci. U.S.A.* 115(5), 921-926 (2018).
- [38] H. R. O. Sohn, P. J. Ackerman, T. J. Boyle, et al., Dynamics of topological solitons, knotted streamlines, and transport of cargo in liquid crystals, *Phys. Rev. E* 97(5), 052701 (2018).
- [39] I. Smalyukh, H. Zhao, and B. Malomed, Topological solitonic macromolecules, *Nature Commun.* 14(1), 4581 (2023).
- [40] A. Vilenkin and E. P. S. Shellard, *Cosmic Strings and Other Topological Defects* (Cambridge University Press, Cambridge, England, 1994).
- [41] S. A. Hojman and F. A. Asenjo, Cosmological electromagnetic Hopfions, *Phys. Scr.* 99(5), 055514 (2024).
- [42] D. Foster, Massive hopfions, *Phys. Rev. D* 83(8), 085026 (2011).
- [43] A. Thompson, A. Wickes, J. Swearngin, et al., Classification of electromagnetic and gravitational hopfions by algebraic type, *J. Phys. A: Math. Theor.* 48(20), 205202 (2015).
- [44] T. Smolka and J. Jezierski, Simple description of generalized electromagnetic and gravitational hopfions, *Class. Quantum Grav.* 35(24), 245010 (2018).
- [45] D. Proment, M. Onorato, and C. F. Barenghi, Vortex knots in a Bose-Einstein condensate, *Phys. Rev. E* 85(3), 036306 (2012).
- [46] H.-B. Luo, L. Li, and W.-M. Liu, Three-Dimensional Skyrmions with Arbitrary Topological Number in a Ferromagnetic Spin-1 Bose-Einstein Condensate, *Sci. Rep.* 9(1), 18804 (2019).
- [47] S. Zou, W.-K. Bai, T. Yang, and W.-M. Liu, Formation of vortex rings and hopfions in trapped Bose-Einstein condensates, *Phys. Fluids* 33(2), 027105 (2021).
- [48] Y. Kawaguchi, M. Nitta, and M. Ueda, Knots in a Spinor Bose-Einstein Condensate, *Phys. Rev. Lett.* 100(18), 180403 (2008).
- [49] D. S. Hall, M. W. Ray, K. Tiurev, et al., Tying quantum knots, *Nat. Phys.* 12(5), 478-483 (2016).
- [50] R. N. Bisset, W. Wang, C. Ticknor, R. Carretero-González, et al., Robust vortex lines, vortex rings, and hopfions in three-dimensional Bose-Einstein condensates, *Phys. Rev. A* 92(6), 063611 (2015).
- [51] T. Ollikainen, S. Masuda, M. Möttönen, et al., Quantum knots in Bose-Einstein condensates created by counterdiabatic control, *Phys. Rev. A* 96(6), 063609 (2017).
- [52] Y.-K. Liu, S.-J. Yang, G.-H. Yang, et al., Interlocked knot in spinor Bose-Einstein condensates, *Chaos, Solitons & Fractals* 140, 110209 (2020).
- [53] B. Jackson, J. F. McCann, and C. S. Adams, Vortex line and ring dynamics in trapped Bose-Einstein condensates, *Phys. Rev. A* 61(1), 013604 (1999).
- [54] W. Wang, R. N. Bisset, C. Ticknor, et al., Single and multiple vortex rings in three-dimensional Bose-Einstein condensates: Existence, stability, and dynamics, *Phys. Rev. A* 95(4), 043638 (2017).
- [55] C. Ticknor, W. Wang, and P. G. Kevrekidis, Spectral and dynamical analysis of a single vortex ring in anisotropic harmonically trapped three-dimensional Bose-Einstein condensates, *Phys. Rev. A* 98(3), 033609 (2018).
- [56] V. P. Ruban, W. Wang, C. Ticknor, et al., Instabilities of a vortex-ring-bright soliton in trapped binary three-dimensional Bose-Einstein condensates, *Phys. Rev. A* 105(1), 013319 (2022).
- [57] M. Abad, M. Guilleumas, R. Mayol, et al., Vortex rings in toroidal Bose-Einstein condensates, *Laser Phys.* 18, 648-662 (2008).
- [58] W.-K. Bai, T. Yang, and W.-M. Liu, Topological transition from superfluid vortex rings to isolated knots and links, *Phys. Rev. A* 102(6), 063318 (2020).
- [59] Y. M. Bidasyuk, A. V. Chumachenko, O. O. Prikhodko, et al., Stable Hopf solitons in rotating Bose-Einstein condensates, *Phys. Rev. A* 92(5), 053603 (2015).
- [60] Y. V. Kartashov, B. A. Malomed, Y. Shnir, et al., Twisted Toroidal Vortex Solitons in Inhomogeneous Media with Repulsive Nonlinearity, *Phys. Rev. Lett.* 113(26), 264101 (2014).
- [61] D. S. Petrov, Quantum Mechanical Stabilization of a Collapsing Bose-Bose Mixture, *Phys. Rev. Lett.* 115(15), 155302 (2015).
- [62] D. S. Petrov and G. E. Astrakharchik, Ultradilute Low-Dimensional Liquids, *Phys. Rev. Lett.* 117(10), 100401 (2016).
- [63] N. B. Jørgensen, G. M. Bruun, and J. J. Arlt, Dilute Fluid Governed by Quantum Fluctuations, *Phys. Rev. Lett.* 121(17), 173403 (2018).
- [64] T. D. Lee, K. Huang, and C. N. Yang, Eigenvalues and Eigenfunctions of a Bose System of Hard Spheres and Its Low-Temperature Properties, *Phys. Rev.* 106(6), 1135-1145 (1957).
- [65] Z. Luo, W. Pang, B. Liu, et al., A new form of liquid matter: Quantum droplets, *Front. Phys.* 16, 1-21 (2021).
- [66] M. Guo, T. Pfau, A new state of matter of quantum droplets, *Front. Phys.* 16(3), 32202 (2021).

- [67] Y. Li, Z. Chen, Z. Luo, et al., Two-dimensional vortex quantum droplets, *Phys. Rev. A* 98(6), 063602 (2018).
- [68] G. Li, Z. Zhao, X. Jiang, et al., Strongly Anisotropic Vortices in Dipolar Quantum Droplets, *Phys. Rev. Lett.* 133(5), 053804 (2024).
- [69] X. Zhang, X. Xu, Y. Zheng, et al., Semidiscrete Quantum Droplets and Vortices, *Phys. Rev. Lett.* 123(13), 133901 (2019).
- [70] Y. V. Kartashov, B. A. Malomed, L. Tarruell, et al., Three-dimensional droplets of swirling superfluids, *Phys. Rev. A* 98(1), 013612 (2018).
- [71] L. Dong, Y. V. Kartashov, Rotating Multidimensional Quantum Droplets, *Phys. Rev. Lett.* 126(24), 244101 (2021).
- [72] Z. Lin, X. Xu, Z. Chen, et al., Two-dimensional vortex quantum droplets get thick, *Commun. Nonlinear Sci. Numer. Simul.* 93, 105536 (2021).
- [73] T. A. Yoğurt, U. Tanyeri, A. Keleş, et al., Vortex lattices in strongly confined quantum droplets, *Phys. Rev. A* 108(3), 033315 (2023).
- [74] G. E. Astrakharchik, B. A. Malomed, Dynamics of one-dimensional quantum droplets, *Phys. Rev. A* 98(1), 013631 (2018).
- [75] C. D’Errico, A. Burchianti, M. Prevedelli, et al., Observation of quantum droplets in a heteronuclear bosonic mixture, *Phys. Rev. Research* 1(3), 033155 (2019).
- [76] I. Ferrier-Barbut, H. Kadau, M. Schmitt, et al., Observation of Quantum Droplets in a Strongly Dipolar Bose Gas, *Phys. Rev. Lett.* 116(21) 215301 (2016).
- [77] R. N. Bisset, L. A. P. Ardila, L. Santos, Quantum Droplets of Dipolar Mixtures, *Phys. Rev. Lett.* 126(2), 025301 (2021).
- [78] L. Dong, M. Fan, B. A. Malomed, Three-dimensional vortex and multipole quantum droplets in a toroidal potential, *Chaos, Solitons & Fractals* 188 115499 (2024).
- [79] H. Hopf, *Selecta Heinz Hopf: Herausgegeben zu seinem 70. Geburtstag von der Eidgenössischen Technischen Hochschule Zürich* (Springer, Berlin, Heidelberg, 1964).
- [80] D. W. Lyons, An Elementary Introduction to the Hopf Fibration, *Math. Mag.* 76(2), 87-98 (2003).
- [81] J. H. C. Whitehead, An Expression of Hopf’s Invariant as an Integral, *Proc. Natl. Acad. Sci. U.S.A.* 33(5), 117-123 (1947).
- [82] L. Faddeev, A. J. Niemi, Partially Dual Variables in SU(2) Yang-Mills Theory, *Phys. Rev. Lett.* 82(8), 1624 (1999).
- [83] J. Jäykkä, J. Hietarinta, P. Salo, Topologically nontrivial configurations associated with Hopf charges investigated in the two-component Ginzburg-Landau model, *Phys. Rev. B* 77(9), 094509 (2008).
- [84] E. Babaev, L. D. Faddeev, A. J. Niemi, Hidden symmetry and knot solitons in a charged two-condensate Bose system, *Phys. Rev. B* 65(10), 100512 (2002).
- [85] J. M. Speight, Supercurrent coupling in the Faddeev-Skyrme model, *J. Geom. Phys.* 60(4), 599-610 (2010).
- [86] J. Jäykkä, J. M. Speight, Supercurrent coupling destabilizes knot solitons, *Phys. Rev. D* 84(12), 125035 (2011).
- [87] Z. Lyu, Y. Fang, Y. Liu, Formation and Controlling of Optical Hopfions in High Harmonic Generation, *Phys. Rev. Lett.* 133(13), 133801 (2024).
- [88] N. G. Vakhitov, A. A. Kolokolov, Stationary solutions of the wave equation in a medium with nonlinearity saturation, *Radiophys. Quantum Electron.* 16(7), 783-789 (1973).
- [89] L. Bergé, Wave collapse in physics: principles and applications to light and plasma waves, *Phys. Rep.* 303(5-6), 259-370 (1998).
- [90] T. G. Skov, M. G. Skou, N. B. Jørgensen, et al., Observation of a Lee-Huang-Yang Fluid, *Phys. Rev. Lett.* 126(23), 230404 (2021).